NeuroImage: Clinical 26 (2020) 101937

Contents lists available at ScienceDirect

NeuroImage: Clinical

journal homepage: www.elsevier.com/locate/ynicl

In search of multimodal brain alterations in Alzheimer's and Binswanger's disease

Zening Fu[a,*], Armin Iraji[a], Arvind Caprihan[a], John C. Adair[b], Jing Sui[a,c], Gary A. Rosenberg[b], Vince D. Calhoun[a,d]

[a] The Mind Research Network, Albuquerque, NM, United States
[b] Department of Neurology, University of New Mexico Health Sciences Center, Albuquerque, NM, United States
[c] Chinese Academy of Sciences (CAS) Centre for Excellence in Brain Science and Intelligence Technology, University of Chinese Academy of Sciences, China
[d] Department of Electrical and Computer Engineering, University of New Mexico, Albuquerque, NM, United States

A B S T R A C T

Structural and functional brain abnormalities have been widely identified in dementia, but with variable replicability and significant overlap. Alzheimer's disease (AD) and Binswanger's disease (BD) share similar symptoms and common brain changes that can confound diagnosis. In this study, we aimed to investigate correlated structural and functional brain changes in AD and BD by combining resting-state functional magnetic resonance imaging (fMRI) and diffusion MRI. A group independent component analysis was first performed on the fMRI data to extract 49 intrinsic connectivity networks (ICNs). Then we conducted a multi-set canonical correlation analysis on three features, functional network connectivity (FNC) between ICNs, fractional anisotropy (FA) and mean diffusivity (MD). Two inter-correlated components show significant group differences. The first component demonstrates distinct brain changes between AD and BD. AD shows increased cerebellar FNC but decreased thalamic and hippocampal FNC. Such FNC alterations are linked to the decreased corpus callosum FA. AD also has increased MD in the frontal and temporal cortex, but BD shows opposite alterations. The second component demonstrates specific brain changes in BD. Increased FNC is mainly between default mode and sensory regions, while decreased FNC is mainly within the default mode domain and related to auditory regions. The FNC changes are associated with FA changes in posterior/middle cingulum cortex and visual cortex and increased MD in thalamus and hippocampus. Our findings provide evidence of linked functional and structural deficits in dementia and suggest that AD and BD have both common and distinct changes in white matter integrity and functional connectivity.

1. Introduction

Alzheimer's disease (AD) is the most common cause of dementia in older individuals (Strittmatter et al., 1993). In the first decade of the 21st century, mortality caused by AD increased by 71%, making AD the sixth leading cause of death in the United States (Alzheimer's, 2015). Vascular cognitive impairment and dementia (VCID), the second most common cause of dementia, has become a major public health concern because of the realization of its impact on the pathogenesis of AD (Corriveau et al., 2016; Kalaria et al., 2008; Rosenberg, 2017; Yin et al., 2014). The most common form of VCID is sub-cortical ischemic vascular dementia (SIVD), which can be divided into two subtypes: Binswanger's disease (BD) and lacunar state. In contrast to lacunar state, BD presents insidiously and follows a slowly progressive course similar to AD (Chui, 2007; Rosenberg et al., 2016). The clinical distinction between AD and BD can be challenging because of their overlapping symptoms as well as their high prevalence in elderly individuals. Therefore, additional neuroimaging features are needed to distinguish these two conditions and make the diagnosis more certain.

Neuroimaging techniques, such as functional magnetic resonance imaging (fMRI), structural MRI (sMRI) and diffusion MRI (dMRI) are more specific and biologically based approaches for detecting brain changes and have been widely employed to probe brain alterations in many brain diseases. White matter (WM) injury on sMRI serves as a prominent brain marker for BD, though about 30% of typical AD patients show similar lesions (Bennett et al., 1990; Bozzali et al., 2002; Delbeuck et al., 2003; Rosenberg, 2017). dMRI assesses WM ultrastructure by quantifying diffusion of water within WM tracts. Mounting evidence has shown dMRI to be more sensitive to WM injury than T2 and fluid-attenuated inversion recovery on sMRI, detecting abnormal diffusion in radiographically normal appearing regions. A wide range of WM abnormalities in both AD and BD have been identified in dMRI studies (Chua et al., 2008; Douaud et al., 2011; Graña et al., 2011; Kantarci et al., 2010). For example, Stahl and colleagues have found that AD patients show reduced fractional anisotropy (FA) in the splenium of the corpus callosum and the temporal lobe (Stahl et al., 2007). FA differences between AD and healthy controls (HCs) were also identified in the bilateral posterior cingulate cortex (PCC) and the

* Corresponding author.
E-mail address: fzn198637@gmail.com (Z. Fu).

https://doi.org/10.1016/j.nicl.2019.101937
Received 28 January 2019; Received in revised form 16 May 2019; Accepted 14 July 2019
Available online 15 July 2019

bilateral superior longitudinal fasciculus (Parente et al., 2008). Studies also identified similar WM abnormalities in BD. A previous study demonstrated that reductions of FA in both regions of the corpus callosum, more in anterior than posterior brain regions in BD patients, suggesting axonal damage and demyelination of fibers (Engelhardt et al., 2009).

fMRI measures brain activity in the gray matter (GM) by evaluating changes associated with blood flow. Investigating resting-state brain functional connectivity from fMRI provides a means for understanding the mechanisms and relevance of the functional relationships between brain regions. AD is characterized by widespread GM changes and disconnection of cortical and sub-cortical regions (Challis et al., 2015; Khazaee et al., 2015; Wu et al., 2013; Zhou et al., 2010). The default-mode network, one of the most widely-studied resting-state networks, is significantly affected by AD. Research has shown that AD patients have decreased resting-state/task activity in the default-mode and hippocampal regions, suggesting disrupted connectivity between these regions (Celone et al., 2006; Greicius et al., 2004). Studies also identified atypical functional connectivity between the hippocampus and several default-mode regions, such as medial prefrontal cortex (mPFC) and PCC (Sorg et al., 2007; Wang et al., 2006). Hence, atypical functional network properties may provide another important biomarker of AD. A recent study combined graph theoretical approaches with machine learning methods to study the AD-related fMRI changes. They showed that three graphic metrics, clustering coefficient, local efficiency, and normalized local efficiency successfully separated patients with AD and healthy controls with 100% accuracy (Khazaee et al., 2015). Although it has also been suggested that resting-state fMRI may provide additional valuable biomarkers of BD (Huisa and Rosenberg, 2014), very limited studies have investigated resting-state functional connectivity in this condition.

Quantitative functional and structural brain alterations have been identified in AD and BD, but many investigations favor one data type only, leaving potentially hidden relationships between different imaging modalities undetected. Therefore, studies of multimodal features are needed to clarify disparate findings in neural imaging (Calhoun et al., 2006; Calhoun and Sui, 2016). During the past decade, increasing studies have used multimodal data to investigate brain changes in AD (Dai et al., 2012; Dyrba et al., 2015; Jung et al., 2015; Prasad et al., 2015). However, these studies typically analyze each modality independently, thus still not evaluating interactions between them. Data fusion is an alternative strategy which analyzes multimodal data jointly and can effectively detect multimodal brain changes related to diseases. The multi-set canonical correlation analysis (MCCA) is one of the promising methods for the exploration of co-impairments in multimodal imaging data. Specifically, it is a data-driven method that decomposes features of each modality into spatial maps (SMs) and their corresponding canonical variants (Li et al., 2009; Sui et al., 2012), and aim to identify co-varying brain patterns among two or more modalities by maximizing the inter-modality correlations between canonical variants. The superior performance of MCCA in achieving jointly associated multimodal components have been shown in comprehensive simulation studies (Correa et al., 2010a, 2010b; Li et al., 2009). Although MCCA is primarily designed to find associations in multi-modalities (Correa et al., 2010a, 2010b; Li et al., 2009), it is also suitable for identifying joint alterations among different modalities in diseases (Lahat et al., 2015; Sui et al., 2012). MCCA has been successfully applied in numerous studies for the exploration of diseases-related multimodal co-alterations. For example, Croitor-Sava et al. have found that the multimodal information captured by this method can contribute to the brain tumor classification (Croitor-Sava et al., 2011). Correa et al. also showed interesting joint alterations between fMRI and gray matter volume using MCCA, with schizophrenia patients having larger functional activity in motor areas and smaller activity in temporal areas (Correa et al., 2008). Sui and her colleagues used MCCA to analyze three types of neuroimaging features from fMRI, sMRI, and dMRI and identified one multimodal component which is not only group differentiating but also highly correlated with the schizophrenic cognitive impairments (Sui et al., 2015). More importantly, their results of this joint component integrated many separated findings in single modality studies (Hoptman et al., 2010; Potkin et al., 2008; Turner et al., 2013). Taken together, the MCCA method is believed to be a powerful tool for finding the potential linkages between multi-modalities and assessing the brain impairments associated with these linked components.

Though multimodal brain changes have been widely studied in many brain disorders, to our knowledge, no report has used fMRI and dMRI data fusion to investigate both commonalities and differences between AD and BD. Understanding the joint changes in different modalities related to AD and BD may advance our knowledge of dementia's mechanism and provide potential multimodal biomarkers for better clinical diagnosis of different dementias. Therefore, in this study, we conducted a fusion analysis to investigate correlated functional and structural brain changes in AD and BD. Results may reveal important joint brain abnormalities which cannot be detected from a single modality.

2. Materials and methods

2.1. Subjects and dataset acquisition

Subjects were collected from an ongoing study of VCID at the University of New Mexico (UNM). In total 124 subjects received MRI scans, including 34 HCs, 18 patients with AD, 16 patients with BD, 11 patients with mixed dementia (AD + BD), 12 patients with leukoaraiosis, 8 patients dementia with Lewy bodies, 8 patients with frontotemporal dementia, 7 patients with Parkinson's disease and 10 patients with psychiatric disorders. HCs were recruited from the community with normal neuropsychological and neurological examinations and patients were recruited from the neurologists' cognitive disorders clinics.

Clinical consensus diagnoses were established after at least one year of clinical follow-up. All patients met the diagnostic and statistical manual of mental disorders (DSM-5R) criteria for dementia (Association, A. P, 2013). Patients diagnosed with AD presented with insidious onset of predominant amnestic disorder associated with one additional cognitive domain, following NINCDS-ADRDA clinical criteria for probable AD (McKhann et al., 1984; McKhann et al., 2011). In addition, they conformed to the recent biological diagnostic criteria for AD, which includes the biomarkers of the AD pathophysiologic process, low cerebrospinal fluid (CSF) $A\beta_{1-42}/A\beta_{1-40}$ and elevated phospho-Tau_{181} (Jack et al., 2018). White matter hyperintensities (WMH) on FLAIR MRI were analyzed by both the semiquantitative visual scale of Fazekas (Fazekas et al., 1987) and the quantitative measurement of WMH volume using an automated program (JIM, http://www.xinapse.com/Manual/). Patients diagnosed with BD met both the Erkinjuntti criteria (Erkinjuntti, 2002) for subcortical vascular dementia and the recent consensus statement for BD (Rosenberg et al., 2016). These patients had predominant dysexecutive syndrome and neurological examination evidence consistent with cerebrovascular injury. All BD patients showed extensive WMH in their MRI scans. Clinical diagnosis of BD was supported in the majority through the absence of AD biomarkers (normal phospho-Tau_{181}). Subjects had been assessed with cognitive tests. Cognitive tests were administered by a trained research psychologist (JP) and trained research coordinators and scored according to standard procedures. Standardized (T) scores were calculated for each test. Average composite T-scores were calculated for five domains (Table 1): memory (Hopkins Verbal Learning Test-Delay, Rey Complex Figure Test-Long Delay), executive function (Digit Span Backwards, Trail Making Test B, Stroop - Interference Score, and Controlled Oral Word Association [FAS]), attention (Digit Span Forward, and Trial Making Test A), language (Boston Naming 60 item test, Controlled Oral Word Association [Animals]) and processing speed

Table 1
Participant demographics.

Phenotypic	HC: Mean (s.d)	AD: Mean (s.d)	BD: Mean (s.d)	*P* value (ANOVA)
Age (61 subjects)	63.94 (8.19)	66.4667 (8.85)	67.40 (6.13)	0.3253
Executive (61 subjects)	51.42 (4.73)	44.79 (7.15)	40.40 (9.08)	6.38e-7
Memory (61 subjects)	53.25 (10.67)	30.93 (9.93)	47.07 (11.23)	6.50e-8
Attention (61 subjects)	52.84 (7.49)	39.80 (10.40)	40.40 (10.77)	6.04e-6
Language (61 subjects)	54.32 (7.55)	42.86 (9.70)	42.67 (8.40)	1.52e-5
Processing Speed (61 subjects)	55.23 (6.55)	43.42 (12.70)	44.27 (9.42)	7.18e-6

(Digit Symbol and Symbol Search, both based on WAIS-3). Research has demonstrated that objective tests should focus on multiple cognitive domains to increase the ability to detect full cognitive impairments (Bondi et al., 2014; Ferman et al., 2013; Loewenstein et al., 2009). We believed that the use of summarized scores for different cognitive domains helps capture more reliable cognitive impairments in dementia.

We included all available subjects 1) with head motion $\leq 3^{\circ}$ and ≤ 3 mm; 2) with functional data providing near full brain successful normalization (detailed procedures are provided in the supplementary materials) for the ICA and the fusion analysis because larger samples provide more a robust and stable estimation of components (Calhoun et al., 2001; Calhoun et al., 2009; Li et al., 2009). These criteria resulted in a total of 113 subjects. Only the HC, AD, and BD groups were further analyzed in subsequent statistical analyses (31 HCs, 15 patients with AD and 15 patients with BD).

2.2. Imaging parameters

Participants were scanned during the eyes-closed rest condition. fMRI Scans were acquired on a 3 T dedicated head scanner (Siemens TIM Trio). Two different head coils were employed during different stages of recruitment, a 12-channel radio-frequency (RF) coil and a 32-channel RF coil with a multi-band sequence. The 12-channel fMRI data were scanned using gradient-echo echo planar imaging (EPI) which had FOV = 240 mm, with a 3.5 mm slice thickness and 30% distance factor, a 3.75 × 3.75 mm in-plane resolution, TR = 2000 ms, TE = 29 ms, anterior-posterior (AP) phase encoding direction, and 165 measurements collected for a total acquisition time of 5.5 min. The 32-channel fMRI data were scanned using a multi-band EPI sequence which had a FOV = 248 mm, 3x3x3 mm voxel resolution, multi-band factor = 8, TR = 460 ms, TE = 29 ms, anterior-posterior phase encoding direction, and 650 measurements collected for a total acquisition time of 5 min. Data for distortion correction were collected using two additional EPI spin-echo sequences run in AP and posterior-anterior (PA) phase encoding directions. The image resolution, echo-spacing, and bandwidth of the EPI fMRI sequence and the EPI spin-echo sequence were matched.

The 12-channel dMRI sequence had 35 gradient directions, b = 800 s/mm^2 and 5 b = 0 measurements for an acquisition time of 6 min. The b = 0 measurements were interleaved after every six non-zero b-value measurements. dMRI data were obtained in the axial direction along the AC–PC line. The FOV was 256 × 256 mm with a 2 mm slice thickness, 72 slices, 128 × 128 matrix size, voxel size = 2 mm × 2 mm × 2 mm, TE = 84 ms, TR = 9000 ms, NEX = 1, partial Fourier encoding of 3/4, and with a GRAPPA acceleration factor of 2. The 32-channel dMRI used a multi-band sequence consisting 165 gradient directions with b-values = 800, 1600, and 2400 s/mm^2, and eight b = 0 values, uniformly distributed over the whole sphere. Data were collected axially with an approximately equal number of volumes in the AP/PA phase encoding directions. The diffusion sequence had 2 mm isotropic resolution with 72 slices, TR = 4000 ms, TE = 108 ms, and a multi-band factor, MB = 3 (13 min).

fMRI preprocessing was performed using a combination of toolboxes: AFNI3 (https://afni.nimh.nih.gov), SPM12 (http://www.fil.ion.ucl.ac.uk/spm/), GIFT4.0b (http://mialab.mrn.org/software/gift), and custom code written in MATLAB. We performed rigid body motion correction using the toolbox in SPM to correct subject head motion, followed by the slice-timing correction to account for timing differences in slice acquisition. Then the fMRI data were despiked using the AFNI3 3dDespike algorithm to mitigate the impact of outliers. The fMRI data were subsequently warped to a Montreal Neurological Institute (MNI) template and were resampled to 3 mm^3 isotropic voxels. All functional images were smoothed using a Gaussian kernel (FWHM = 6 mm). For the 32-channel fMRI data, additional distortion correction was conducted. A distortion field was calculated from the AP and PA phase-encoded EPI data by the TOPUP/FSL algorithm (Andersson et al., 2003). This distortion field was then used to correct the fMRI images. This was followed by motion correction and spatial normalization steps. Based on the 6 realignment parameters, we calculated the mean of the absolute translation and the mean of the absolute rotation for the selected subjects. We compared these head motion parameters among groups using analysis of variance (ANOVA). The results show that there is no group difference on the head motion (translation: $p = .1566$; rotation: $p = .2131$).

dMRI preprocessing was similar for the 12-channel and the 32-channel RF coil data. The preprocessing steps consisted of a) Distortion and Motion correction and b) Quality control check. The data processing was primarily based on the FSL software (//fsl.fmrib.ox.ac.uk) with a custom MATLAB routine for quality check. The distortion correction methods were different for the two coils data sets. In the case of the 32-channel RF coil, the diffusion data was collected in the AP and the PA phase encoding directions. We first estimated the distortion field by the TOPUP/FSL routine based on the reversed phase encoding diffusion data. Then EDDY/FSL together with the distortion field was applied to correct for distortion as well as motion related artifacts. This ability to calculate the distortion field was not available for the 12-channel data. In this case, the FLIRT/FSL algorithm with 12 degrees of freedom, affine transformation, and mutual information as the cost function was used for motion correction by registering the images to the first b = 0 image. This was followed by a MATLAB routine which checked for signal dropout because of motion and/or the presence of excessive motion as reported by the motion correction algorithm. A subject was excluded from further analysis if it had > 10% of bad volumes. Similar to fMRI, we compared the mean of the absolute translation and the mean of the absolute rotation among groups and found no group difference on the head motion (translation: $p = .3511$; rotation: $p = .6222$).

2.3. Feature extraction

2.3.1. fMRI feature

Functional network connectivity (FNC) between components was calculated and used as the fMRI feature. Spatial GICA was performed on preprocessed fMRI data to define the regions of interest. Principal components analysis (PCA) was firstly performed on each subject to reduce subject-specific data into 120 principal components which preserve > 99% of the variance. Secondly, the first level reduced data were concatenated and then reduced to 100 principal components using expectation maximization algorithm (Erhardt et al., 2011). Thirdly, the infomax algorithm was used to decompose the second level reduced

group data into 100 independent components (ICs) and estimate the group level spatial maps (SMs). ICASSO was applied on 20 ICA runs and the best-run was chosen to stabilize the estimation (Ma et al., 2011). ICASSO is a software package which is capable of investigating the relations between estimates from ICA (Himberg and Hyvarinen, 2003). The SMs and their corresponding time-courses (TCs) were back-reconstructed based on the group SMs using a spatially constrained algorithm called group information guided ICA (GIG-ICA) (Du et al., 2016; Du and Fan, 2013). We selected a relatively high model order (number of ICs, C = 100) for the functional parcellation of brain components to probe more detailed inter-connected information of the functional regions. Using such a high model order is consistent with our previous static and dynamic FNC studies in other brain disorders (Damaraju et al., 2014; Fu et al., 2017; Fu et al., 2018; Rashid et al., 2016; Rashid et al., 2014).

After obtaining subject-specific SMs and TCs of all ICs, one-sample *t*-test maps for each SM and the mean power spectra of each TC were computed. We chose a set of ICs that cover the majority of sub-cortical and cortical GM as intrinsic connectivity networks (ICNs) for FNC feature extraction by visual inspection using the same criteria described in our previous studies (Allen et al., 2014; Damaraju et al., 2014; Fu et al., 2018; Rashid et al., 2016). That is, those components identified as ICNs should exhibit peak activations in gray matter, low spatial overlap with known vascular, ventricular, motion, and susceptibility artifacts, and should have TCs dominated by low-frequency fluctuations (Allen et al., 2014). The selected ICNs were categorized into different functional domains according to anatomy and prior knowledge of their function. We defined additional hippocampal domain because we want to highlight the hippocampal regions that are typically involved in dementia studies. It should be noted that the organization of different ICNs into different functional domains is just used for better visualization of the results and does not have any influence on the fusion analysis. Before calculating the FNC between ICNs, the following post-ICA processing steps were conducted on the TCs to remove remaining noise sources: 1) detrending linear, quadratic, and cubic trends; 2) conducting multiple regressions of the 6 realignment parameters and their temporal derivatives; 3) de-spiking detected outliers; 4) low-pass filtering with a cut-off frequency of 0.15 Hz. The Pearson correlation coefficient between TCs was calculated after post-processing as the measure of the fMRI feature.

2.3.2. dMRI feature

The fractional anisotropy (FA) and the mean diffusivity (MD) maps were calculated by the DTIFIT/FSL algorithm. The FA images were non-linearly spatially normalized to an FA MNI template (FNIRT/FSL) and then this transformation was also applied to the MD images to transform them to the MNI template. This resulted in a 91x109x91 matrix with the voxel size of 2x2x2 mm for FA and MD maps. The FA and MD maps were smoothed using a Gaussian kernel (FWHM = 6 mm) before the fusion analysis.

2.4. Fusion analysis

Since the data were scanned using two different head coils, before the fusion analysis, we corrected the head coil effect from the fMRI and dMRI features. Among 113 subjects used in the fusion analysis, 76 subjects (including 20 HCs, 13 AD patients, 6 BD patients, and 37 other patients) were scanned with a 32-channel RF coil and 37 subjects (including 11 HCs, 2 AD patients, 9 BD patients, and 15 other patients) were scanned with a 12-channel RF coil. A generalized linear model (GLM) was applied to the features of 31 HCs to estimate the effect of the different head coils. We used only the features from HC for the estimation to avoid confounding effects related to diseases. After obtaining the effect of head coils, we regressed out this effect from all subjects. The confounding effect of head coils was removed from each feature (FNC, FA, and MD).

Next, FA and MD feature masks were created to extract significant dMRI features for fusion analysis. That is, for the FA feature, we calculated the individual mask for each subject by setting voxels which are > 90% of the whole brain mean to 1. Next, we computed a feature mask for all subjects by setting voxels which are included in > 90% of the subjects to 1. For the MD feature, we generated a feature mask by excluding the ventricles and other possible CSF regions. The 2D FNC feature and the 3D dMRI features (FA and MD inside the feature masks) of each subject were reshaped into a one-dimensional non-zero vector and stacked one by one, forming a matrix with dimensions of subject x [number of features] for each feature, respectively. To make different features into the same range with the same average sum of squares, the feature matrix was normalized. We used a single normalization factor for each feature to guarantee that the relative scaling within a feature was preserved, but the units between features were the same (Sui et al., 2011).

The normalized features were jointly analyzed by MCCA, which is capable of characterizing the linked patterns among different features. Research has shown that MCCA can detect flexible co-occurring abnormalities from different modalities and is a powerful tool to provide additional information of brain disorders which cannot be captured in single modality analysis (Correa et al., 2008; Li et al., 2009; Sui et al., 2015). The flowchart of the MCCA approach is displayed in Fig. 1. MCCA is an extension of traditional CCA method which is used to find the optimal transformed coordinate system which can maximize the correlation between the canonical variants of different data features. Different from two-way CCA, MCCA is a multiple-stage optimization method which explores the linear combination of components that maximizes the correlations between canonical variants in each stage (Li et al., 2009). Consistent with our previous studies, we used the modified minimum description length (MDL) criterion to estimate the number of components for each feature (FNC, FA, and MD) (Li et al., 2007). The final component number for fusion analysis was set as the maximum value of the estimated component number for each feature, which maximally retains the joint information (Sui et al., 2013).

2.5. Correlation analysis and group difference detection

The association between canonical variants of paired-features was measured by the Pearson correlation coefficient. A permutation test was conducted to mitigate against overfitting. We permutated each feature across subjects and then performed MCCA on the permutated data 2000 times. Then we calculated the correlation between canonical variants to generate the null distribution. If the correlations between canonical variants of components (regressed out the group label information) from the original data are larger than 95% of the correlations between canonical variants from the permutated data, we set these components as components of interest (COIs). ANOVA was performed on HC, AD, and BD groups for each canonical variant of COIs (control covariates: age and gender). If the ANOVA results show significant group difference in canonical variants, a GLM was applied to examine the effect of diagnosis on each canonical variant of COIs (control covariates: age and gender) between pairs of groups (HC vs. AD, HC vs. BD, and AD vs. BD).

3. Results

3.1. Spatial maps of identified intrinsic connectivity networks

The resulting SMs of ICNs are displayed in Fig. 2. Among 100 estimated ICs, 49 of them were identified as ICNs and arranged into 8 different groups based on their anatomical and presumed functional properties: sub-cortical domain (SC), hippocampal domain (HIP), auditory domain (AUD), visual domain (VIS), sensorimotor domain (SEN), cognitive-control domain (CC), default-mode domain (DM), and cerebellar domain (CER). Our manual organization of ICNs is similar to the ordering results obtained by various empirical methods, such as

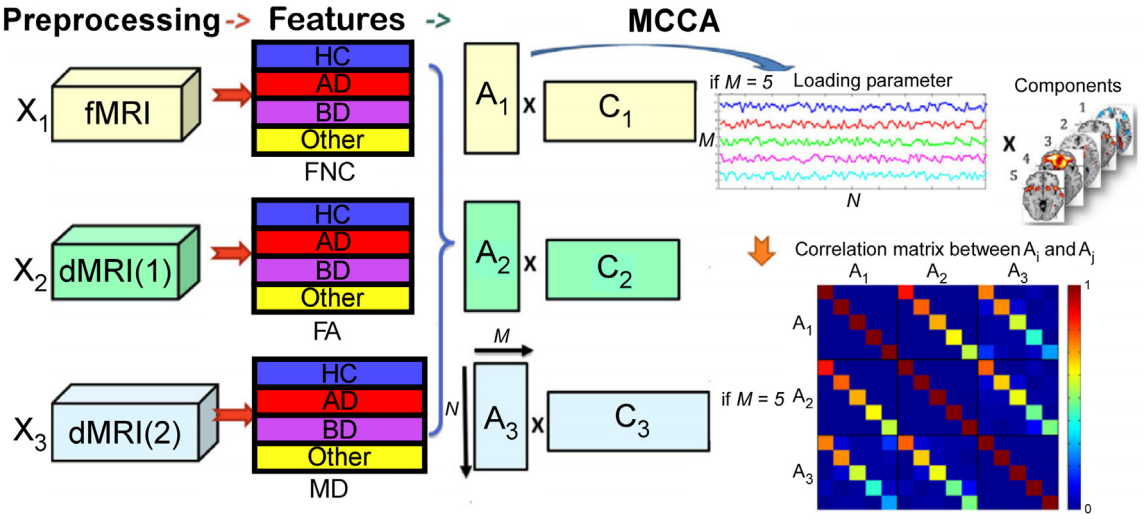

Fig. 1. Flowchart of the multi-set canonical correlation analysis (MCCA) on multiple features, which enabels capturing multimodal alterations. Step 1: extract functional network connectivity (FNC) features from fMRI data and fractional anisotropy (FA)/mean diffusivity (MD) features from dMRI data; Step 2: run MCCA method on these features. The MCCA optimizes an objective function of the correlation matrix of the canonical variants from multiple random vectors such that the canonical variants achieve maximum overall correlation. The MCCA will separate each feature into canonical variants (A_i) and spatial maps (C_i) and the canonical variants will have high correlations across modalities. In our present study, the feature matrix of each modality is decomposed into 26 canonical variants and 26 corresponding spatial maps (SMs), M = 26. The canonical variants represent how the components distributed in participants. AD, Alzheimer's disease; BD, Binswanger's disease.

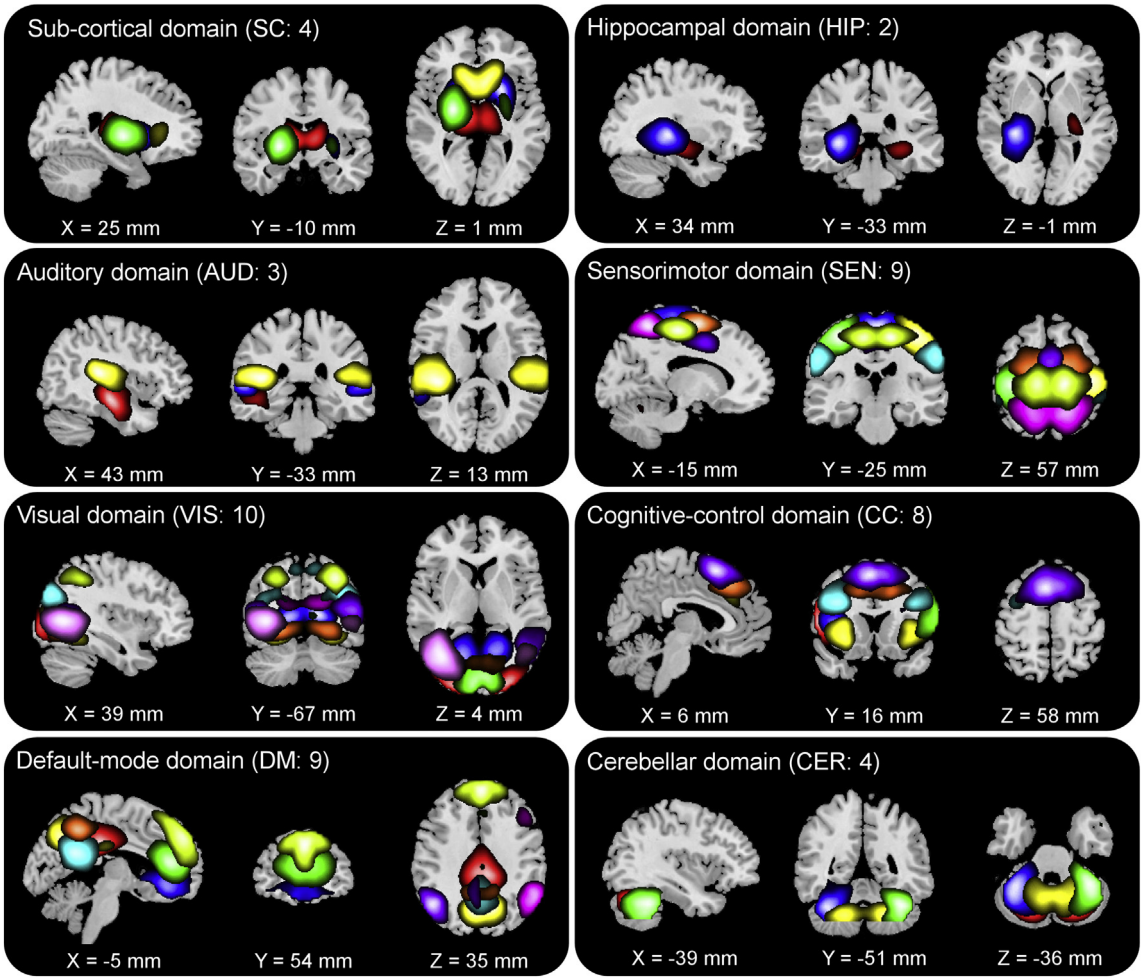

Fig. 2. Spatial maps (SMs) of the 49 identified intrinsic connectivity networks (ICNs), arranged into eight functional domains. The number of ICNs arranged to each functional domain is provided. Each color in the SMs corresponds to a different ICN. Components labels and peak coordinates are provide in Table S1.

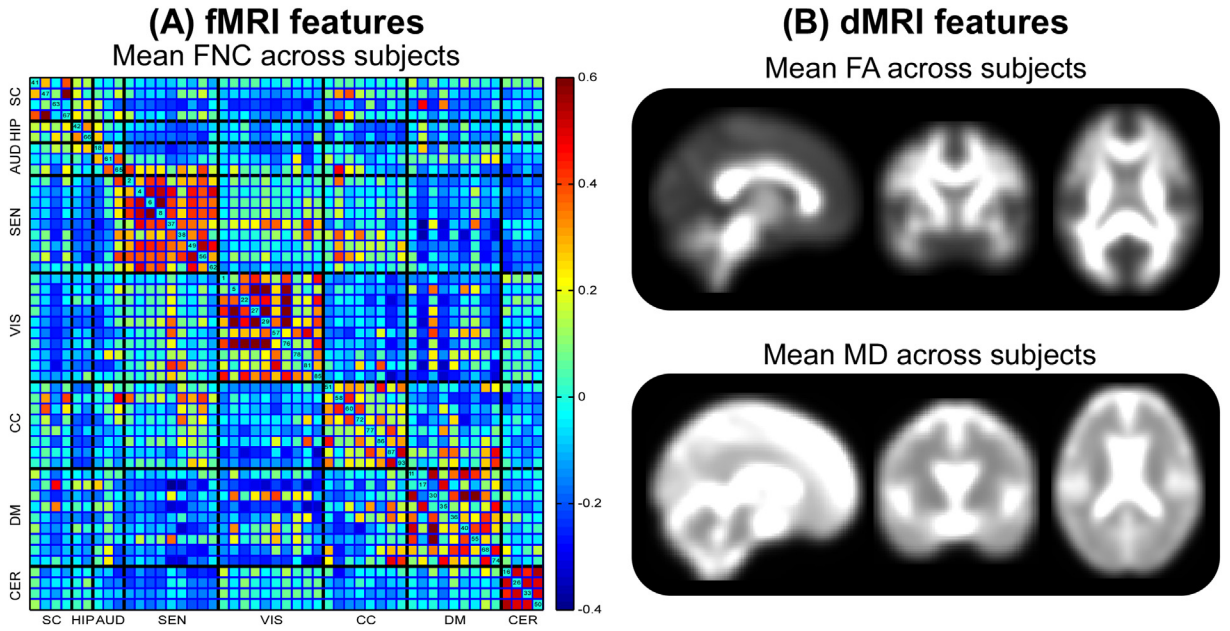

Fig. 3. Mean of functional network connectivity (FNC) feature, fractional anisotropy (FA) feature, and mean diffusivity (MD) feature across subjects. FNC is caculated by Pearson correlation coefficient between time-courses (TCs) of indepenedent components (ICs). FA and the MD maps were calculated by the DTIFIT/FSL algorithm.

spectral clustering and modularity optimization (Allen et al., 2014; Rubinov and Sporns, 2010).

3.2. Feature maps of fMRI and dMRI

We calculated FNC between ICNs as the fMRI feature and voxel-wise FA and MD maps as the dMRI features for fusion analysis. The mean FNC, mean FA and mean MD across all subjects are displayed in Fig. 3. It can be observed that ICNs from the same functional domain are highly correlated with each other while ICNs from different functional domains are less correlated or even negatively correlated. We can also observe clear patterns of fiber density and myelination in WM from the FA map and the patterns of water diffusion within brain tissue from the MD map.

3.3. Joint components of interests

The number of components estimated using modified MDL was 26, 18, and 22 for the FNC feature, FA feature and MD feature respectively. Therefore, we chose $M = 26$ for fusion analysis. Although MCCA was conducted on the extracted features of interest, for the $M = 26$ case, a considerable amount of variance was still retained for each feature (95% for FNC, 98% for FA and 97% for MD). We aimed to investigate significant joint components of these three features and to explore whether the joint components discriminate between groups. Among the 26 derived joint components, the first ten components passed the permutation test ($p < .05$, false discovery rate (FDR) corrected). After regressing out the label information from the canonical variants, we found that the correlations between the canonical variants of the first two components still pass the permutation test ($p < .05$, FDR corrected). The canonical variants of these two joint components are significantly different between groups. The canonical variants of the first component show significant differences between AD and HC ($p = 7.15 \times 10^{-4}$, 0.0126, 0.0282 for FNC, FA and MD respectively, FDR corrected), between AD and BD ($p = .0215$, 0.0121, 0.0089 for FNC, FA and MD respectively, FDR corrected), and between BD and HC ($p = .0343$ for MD, FDR corrected). The canonical variants of the second component show significant differences between BD and HC groups ($p = .0204$, 4.93×10^{-4}, 2.03×10^{-5} for FNC, FA and MD respectively, FDR corrected), and between AD and BD ($p = .0071$, 0.0067, 0.0022 for FNC, FA and MD respectively, FDR corrected). Fig. 4 displays the SMs of the first component, which were adjusted according to the box plots shown in Fig. 5. The red regions/links in subplots (A) and (C) of Fig. 4 indicate higher values in AD than in HC/BD and the blue regions/links in subplots (B) and (C) indicate higher values in HC/BD than in AD. In subplot (D) of Fig. 4, the red regions indicate a relationship that AD > HC > BD and the blue regions indicate a relationship that AD < HC < BD. Similarly, Fig. 6 displays the SMs of the second component, in which the red regions/links indicate higher values in BD than in HC/AD and the blue regions/links indicate higher values in HC/AD than in BD. For each component, the SMs are transformed into Z scores and visualized at a given threshold ($|Z| > 2$), where the highlighted regions have relatively more contribution to this component (Li et al., 2009; Sui et al., 2012) and are supposed to be impaired in the patient groups if the corresponding canonical variants show significant group difference.

It should be noted that, although the difference between BD and HC in the first component (i.e., significant for MD feature only) and the difference between AD and HC in the second component are modest, the AD and BD groups exhibit distinct alteration patterns for both components. For the first joint component, the AD and BD groups show changes in opposite directions (compared with the HC group, the canonical variants of the AD group increased while the canonical variants of the BD group decreased). In contrast, for the second joint component, the AD and BD groups generally have similar brain changes but with different degrees (compared with the HC group, the canonical variants of the AD and the BD groups both increased in FA and MD). As displayed in Figs. 5 and 7, the canonical variants of different features remain highly correlated even after regressing out group labels.

The SMs of the first component show that AD has lower FA in body, genu, and splenium of corpus callosum. No area of increased FA is observed. AD has higher MD in the medial superior frontal cortex, superior temporal cortex, and temporal pole, and lower MD in the left superior frontal cortex. Interestingly, BD shows opposite MD changes in these brain regions. The observed dMRI patterns are highly correlated with changes in FNC. FNC between the cerebellum and DM and VIS domains increases in AD while FNC involving the temporal pole, thalamus and hippocampus decreases.

The SMs of the second component show that BD has higher FA in the middle cingulate cortex (MCC), PCC, precuneus, lingual gyrus and

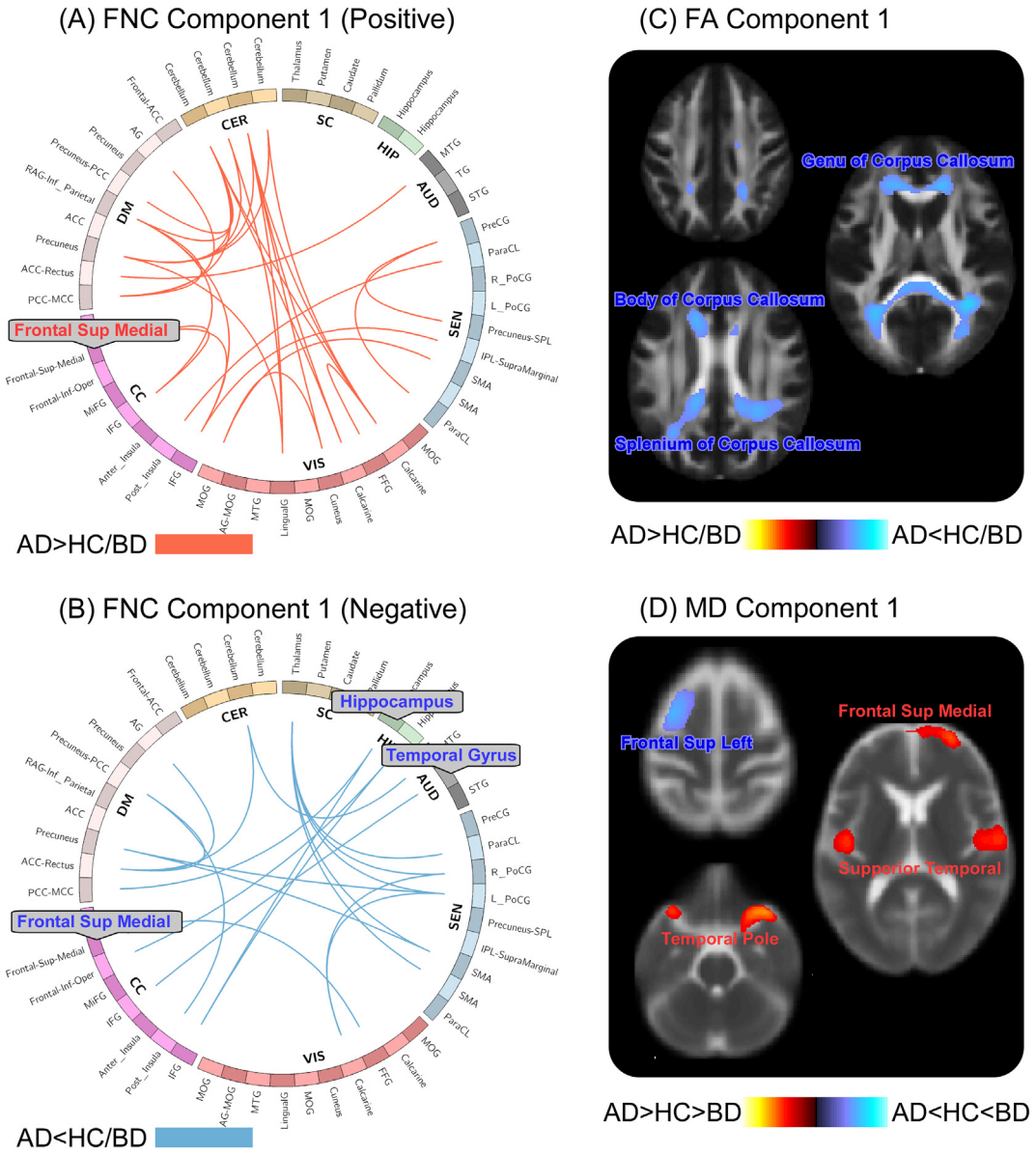

Fig. 4. Spatial maps (SMs) of joint component 1 that are significantly group-discriminating. (A)-(B) functional network connectivity (FNC); (C) fractional anisotropy (FA); (D) mean diffusivity (MD). The SMs visualized at $|Z| > 2$. The positive values in (A) and (C) represent Alzheimer's disease (AD) > healthy control (HC)/ Binswanger's disease (BD), while the positive values in (D) represent AD > HC > BD. The negative values in (B) and (C) represent AD < HC/BD, while the negative values in (D) represent AD < HC < BD.

cerebral peduncles, and lower FA in anterior corona radiata, internal capsule, and posterior thalamic radiations. Moreover, the BD group has significantly increased MD in Heschl's gyrus, hippocampus, middle temporal cortex, and thalamus. These structural brain changes are associated with increased MCC/PCC related between-domains FNC and decreased MCC/PCC related within-domain FNC. Thalamus and lingual gyrus involving between-domains FNC also decreases in the BD group.

4. Discussion

In this paper, we investigated brain co-alterations from two modalities (fMRI and dMRI) across three diagnostic groups (HC, AD, and BD). To our knowledge, this is the first study to clarify AD and BD related brain changes in different MRI modalities via a functional-structural data fusion model. Note that the joint components with group-discriminating canonical variants do not mean that all regions that contribute to the component are significantly impaired. We transformed the SMs into Z scores and highlighted those regions with relatively more contribution to the components ($|Z| > 2$), which are more likely to be impaired in patients. We found that 1) brain changes in fMRI FNC, dMRI FA, and dMRI MD are highly correlated with each other; 2) AD and BD share both similar and different (and in some cases opposite) functional and structural brain changes. The overall results demonstrate that investigating multimodal brain imaging data through fusion analysis might help to capture more brain disorders relevant information and advance our knowledge of the relationships between functional and structural abnormalities in the brain.

4.1. Distinct functional and structural brain co-alterations in AD and BD

The SMs of the first component displayed in Fig. 4 show distinct brain alteration trends between AD and BD groups. Both increased and decreased cerebellar FNC is observed in the AD group. The cerebellum is connected to many brain networks and contributes to complex brain functions, such as cognitive and sensorimotor processing (O'reilly et al., 2009; Schmahmann et al., 2007). Previous studies have shown that the

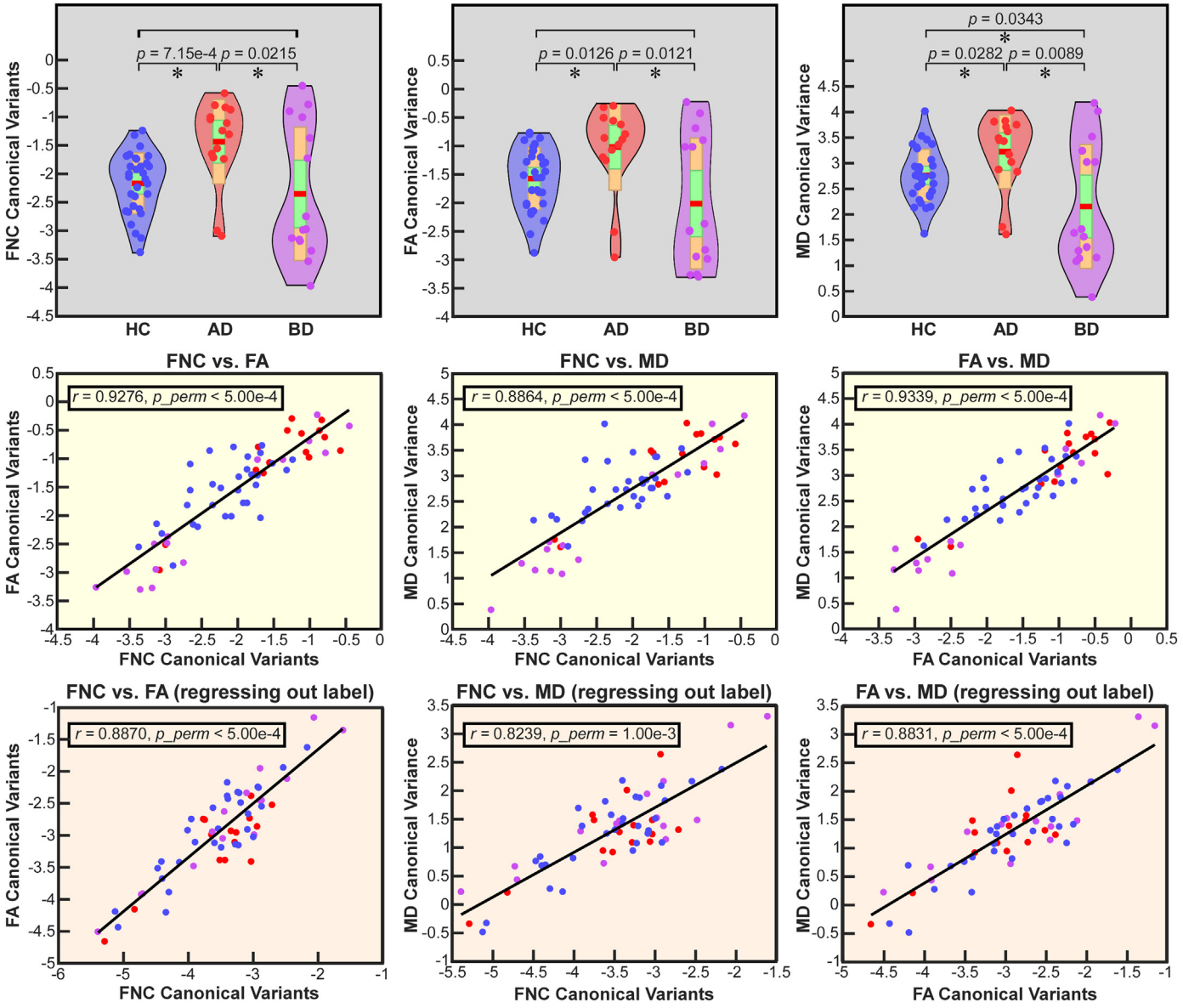

Fig. 5. Group comparisons of canonical variants of joint component 1 and correlations between canonical variants. Top row: boxplot of canonical variants of each feature component, with *p* values of generalized linear model (GLM) test between pair-groups(stars indicate significant group difference after False discovery rate [FDR] correction). Middle row: Pearson correlations between canonical variants of each feature component and p values of the permutation test. Bottom row: Pearson correlations between canonical variants of each feature component after regressing out group labels and p values of the permutation test. FNC, functional network connectivity; FA, fractional anisotropy; MD, mean diffusivity; HC, healthy controls; AD, Alzheimer's disease; BD, Binswanger's disease.

cerebellar functional connectivity is affected by dementias (Bai et al., 2011; Castellazzi et al., 2014), especially AD, and such abnormalities are associated with cognitive decline (Zheng et al., 2017). However, the findings in cerebellar connectivity are inconsistent and even contradictory to some extent, since both increased and decreased cerebellum related functional connectivity have been identified in AD (Castellazzi et al., 2014; Zheng et al., 2017). Our current study performed ICA decomposition using a high model order which can provide more detailed functional parcellation of the brain. Both increased and decreased CER related FNC is identified in AD patients, suggesting that cerebellar connectivity might have different abnormalities and the definition of the regions of interest might be a possible source of previous disparities. The superior medial frontal gyrus also shows atypical FNC in the AD group, especially with inferior frontal gyrus (IFG), which is consistent with previous findings on dorsolateral prefrontal cortex (DLPFC) connectivity in AD (Allen et al., 2007; Park et al., 2016; Wang et al., 2006). DLPFC is highly associated with many cognitive functions which are commonly affected in AD. The identified increased FNC within the CC domain might support the hypothesis that AD patients recruit more resources in the prefrontal cortex to compensate for cognitive function loss (Grady et al., 2003). Decreased hippocampus FNC (e.g. FNC between hippocampus and PCC) is found in our study as well, which is also compatible with the disconnection hypothesis (Wang et al., 2006).

Identified WM changes in the AD group are mainly located in DLPFC, temporal cortex, and corpus callosum. AD patients have significantly decreased FA in genu, body, and splenium of corpus callosum. Similar findings have been reported in previous work on AD (Douaud et al., 2011). Atypical FA in corpus callosum has been shown to be a useful measure for monitoring disease progression (Acosta-Cabronero et al., 2012). It is argued that axon loss in the corpus callosum, a region of usually high anisotropy, will result in a decrease in the FA of that region (Rose et al., 2000). Wallerian degeneration of these WM fiber tracts secondary to axon loss is assumed to be a major contributing factor of WM changes in AD (Bozzali et al., 2002). Our

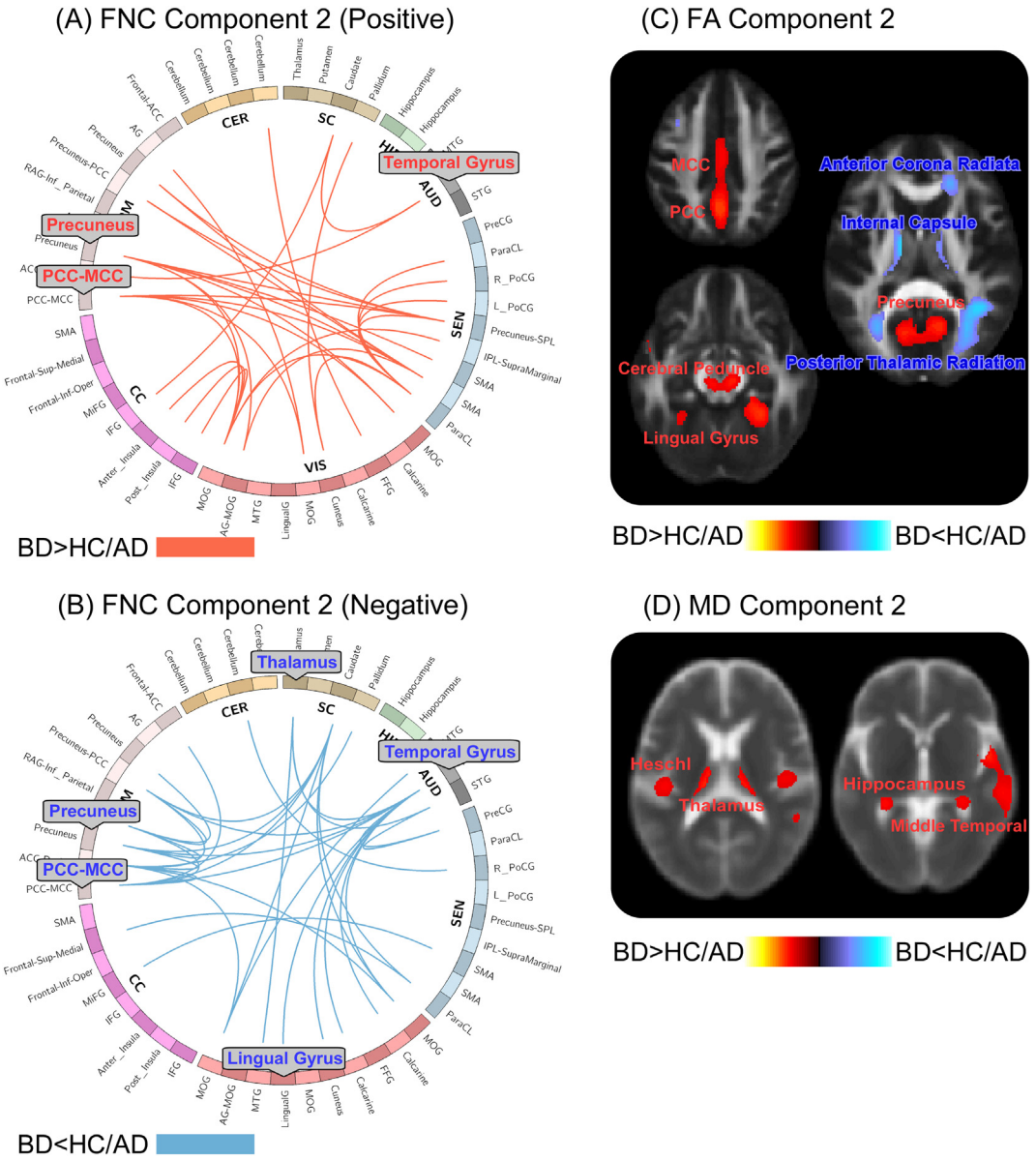

Fig. 6. Spatial maps (SMs) of joint component 2 that are significantly group-discriminating. (A)-(B) functional network connectivity (FNC); (C) fractional anisotropy (FA); (D) mean diffusivity (MD). The SMs visualized at $|Z| > 2$. The positive values represent Binswanger's disease (BD) > healthy control (HC)/Alzheimer's disease (AD), while the negative values represent BD < HC/AD.

results are in line with these findings and further show that the FA changes in AD are highly associated with changes in functional brain connectivity. These associations might reveal potential relationships between WM ultrastructural damages and functional brain disconnections in dementia.

Increased MD in AD is detected in the superior medial frontal gyrus, superior temporal gyrus (STG) and temporal pole. MD is a common measure of translational diffusion, which increases in the presence of tissue damage (Stebbins and Murphy, 2009). MD is suggested to be a sensitive marker of neurodegeneration related to AD (Henf et al., 2018). Previous studies have documented a wide range of increased MD in AD, especially in temporal lobes and frontal lobes (Bozzali et al., 2002; Salat et al., 2010; Stahl et al., 2007). Our results demonstrate that MD can have distinct changes in different cortical regions (both increased and decreased MD were observed in the AD group), which might underlie different tissue alterations in AD. It should be noted that the temporal and frontal cortex show both functional and structural changes in the AD patients and such co-alterations might indicate responses to brain system injury to, at least temporarily, remediate network organization to maintain task performance (Bookheimer et al., 2000; Grady et al., 2003). Another interesting observation in our current study is that AD group and BD group have opposite MD changes in the temporal and frontal cortex. Such differences between AD and BD groups suggest that dysfunction in AD and BD may be caused by distinct types of WM damage.

4.2. Similar functional and structural brain co-alterations in AD and BD

The results in Figs. 6 and 7 show that AD and BD patients also share similar brain alterations, but such alterations are more severe in the BD group. FNC between DM and some sensory regions (e.g. regions within VIS and SEN) increases while FNC within DM decreases in the BD group. Since DM is anti-correlated with the sensory domains, the higher correlations represent the weaker negative FNC (closer to zero). In that case, the atypical DM FNC reveals the diminished connections with the DM in BD. DM and its functional connectivity are associated with aging

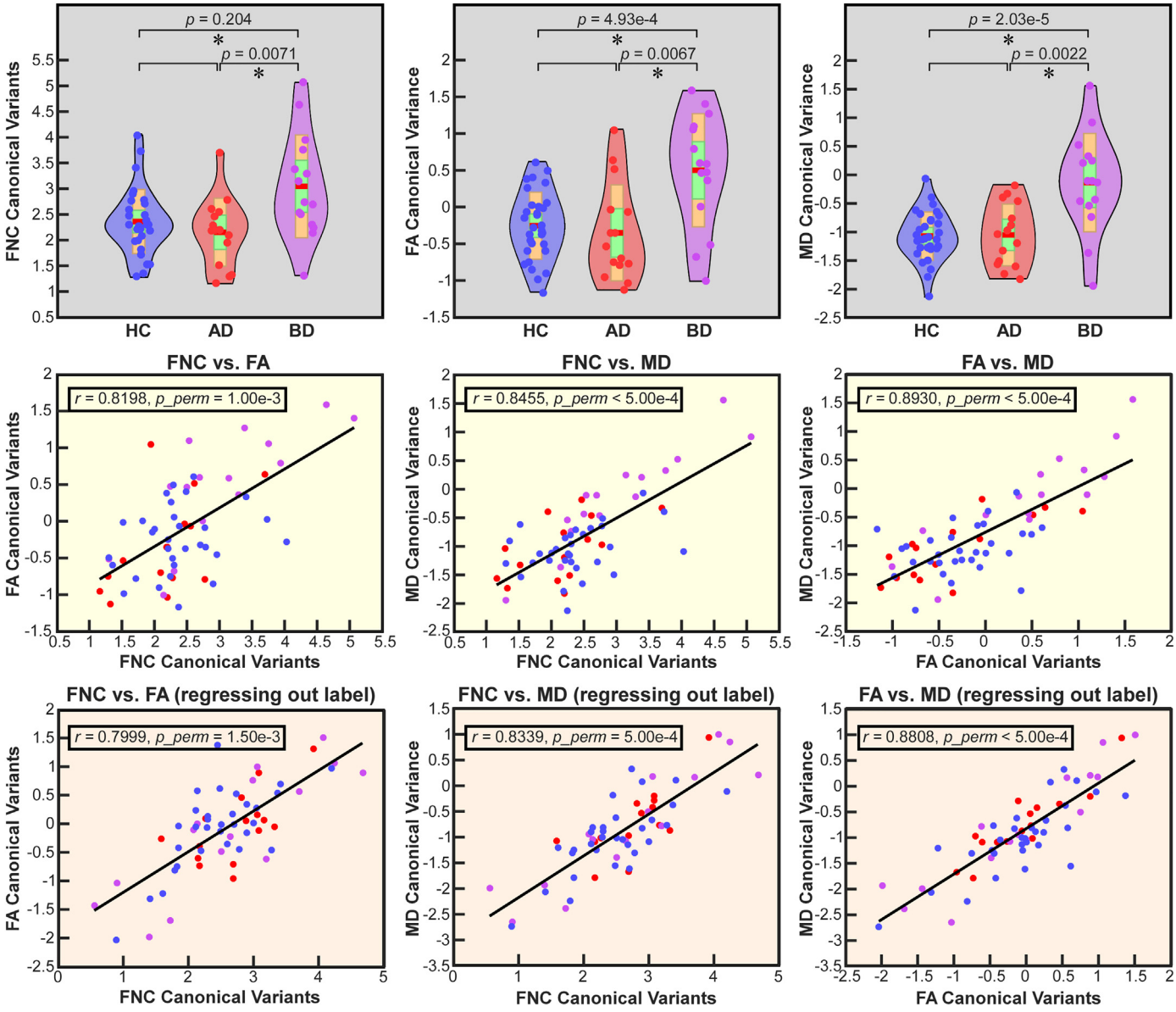

Fig. 7. Group comparisons of canonical variants of joint component 2 and correlations between canonical variants. Top row: boxplot of canonical variants of each feature component, with p values of generalized linear model (GLM) test between pair-groups(stars indicate significant group difference after False discovery rate [FDR] correction). Middle row: Pearson correlations between canonical variants of each feature component and p values of the permutation test. Bottom row: Pearson correlations between canonical variants of each feature component after regressing out group labels and p values of the permutation test. FNC, functional network connectivity; FA, fractional anisotropy; MD, mean diffusivity; HC, healthy controls; AD, Alzheimer's disease; BD, Binswanger's disease.

and are also highly affected by AD (Agosta et al., 2012; Jones et al., 2011; Wang et al., 2007; Wang et al., 2006). AD patients have been reported both decreased positive functional connectivity within DM and decreased negative functional connectivity (less negative, closer to zero) between DM and its anti-correlated networks (Klaassens et al., 2017; Wang et al., 2006). Such disconnection between DM and the other brain regions has been interpreted by decreased resting-state DM activity (Greicius et al., 2004). The identified increased PCC-MCC FA in the current study might imply decreased DM GM activations in the patients' groups. Therefore, the positive correlation between decreased DM FNC and increased DM FA extends the disconnection hypothesis (Greicius et al., 2004) by showing that functional disconnections might be mediated through WM damage. Paracentral lobule involved FNC also shows significant changes (both increased and decreased FNC with different brain regions) in the BD group. Recent research has reported increased paracentral lobule functional connectivity in AD (Tucholka et al., 2018; Zhao et al., 2018). Our results highlight that distinct FNC changes in the paracentral lobule may be more associated with dementia in BD.

AD and BD patients share similar structural brain changes in some other brain regions besides those DM regions (PCC-MCC and precuneus). Compared with the HCs, patients have decreased FA in anterior corona radiate, internal capsule, and posterior thalamic radiation. Decreased FA in posterior thalamic radiation has been widely reported in AD (Mayo et al., 2017; Zhu et al., 2015). Our results are in line with these previous findings and further show that BD patients have more FA changes in these brain regions, which might be associated with more severe WM damages. BD patients also show increased FA in lingual gyrus and cerebral peduncle. Lingual gyrus has been demonstrated to be highly related to age (Ibrahim et al., 2009) and AD (Yetkin et al., 2006). The degraded linguistic abilities in some AD patients are reported, even before the onset of the disease (Garrard et al., 2004; Venneri et al., 2008). The observed atypical FA in lingual gyrus reveals that such brain damage may be common in BD patients, suggesting that

BD might also result in degraded linguistic abilities.

The thalamus and middle temporal gyrus have significant increased MD, but decreased FNC between them, especially in BD patients. Increased MD indicates tissue structural damage in these regions, which might further result in alterations of structural connections between them. Previous studies have combined resting-state fMRI with dMRI to demonstrate that resting-state functional connectivity reflects a large degree of underlying structural connectivity (Greicius et al., 2009). Therefore, damage to WM might result in both changes in MD through the loss of barriers to free diffusion (Stebbins and Murphy, 2009) and changes in functional connectivity through the alterations of structural connections. AD and BD patients have increased MD in some other regions, including Heschl's gyrus and hippocampus. Hippocampus is one of the major neural structures involving episodic memory, which is severely impaired by AD and other dementias (Rosenberg, 2017; Soininen and Scbeltens, 1998). The MD value of hippocampus is a sensitive measure of early degeneration in AD and it has great discriminating power between AD and normal aging (Kantarci et al., 2001; Kavcic et al., 2008; Li et al., 2013; Rose et al., 2008; Stebbins and Murphy, 2009). Our current study reveals the presence of hippocampus MD alterations in both AD and BD (although it is only significant for BD), suggesting hippocampus WM changes to be a common cause of memory impairments in different types of dementia.

5. Potential limitations and future directions

In this study, we used GICA and MCCA to investigate multimodal brain alterations in AD and BD. GICA and MCCA are two data-driven decomposition approaches that identify brain components based on the co-varying patterns of the brain. One limitation of our study is the relatively small sample size of the targeted groups (HC, AD, and BD). Therefore, we have taken careful steps to maximize reliability. First, we used all available subjects, including HC, AD, BD, and the other patients in the GICA. Previous studies have shown that individual subject results are well captured within GICA (Allen et al., 2012; Du and Fan, 2013). The identified ICNs in the present studies are highly consistent with previous high-model order ICA studies (Allen et al., 2014; Damaraju et al., 2014; Fu et al., 2017; Fu et al., 2018), indicating that the defined components are very common and not biased by specific types of brain disorders. We also provided GICA results using only the targeted groups (61 subjects) in the supplementary materials and the overall results supported our arguments that more subjects in the GICA can provide more reliable estimates and the FNC features are not biased by the other patient groups. Second, we included all subjects with good data quality in the MCCA for capturing reliable co-varying components. We performed a permutation test for identifying the components of interesting. The results showed that, although the joint components were estimated using all available subjects, significant inter-modalities correlations were observed within the target groups, even the group labels have been regressed out (passed the permutation test, FDR corrected). These results demonstrated that identified joint components capture the real inter-subjects co-variability of the targeted subjects, which is not influenced by the group labels and the overfitting of the fusion method. Third, we regressed out age, gender, and head coil effects during the analysis to remove any potential confounding effects that might have influences on the results. We view this study as the discovery phase for potential biomarkers because all the analysis in this study can be easily implemented to compute features from new coming subjects, and this provides an attractive framework going forward for leveraging and applying the identified neuroimaging features to new data.

This manuscript is based on a dataset collected from an ongoing VCID study, in which new subjects are continuously recruited. Therefore, we would like to validate our current observations using more subjects in the future. Another limitation is our current study only focused on the statistical difference among groups. Whether such group differences are valuable biomarkers for clinical diagnosis should be considered and investigated in future studies with more subjects and greater statistical power. Patients with psychiatric diseases are used in the GICA and the fusion analysis but are not investigated through statistical analysis because of the limited number of subjects ($\leq$ 8 after subject selections). We can extend our analysis to search for potential multimodal brain alterations for psychiatric diseases when more subjects with psychiatric diseases have been recruited.

6. Conclusion

In this study, we used a multivariate method to investigate brain co-alterations in AD and BD. This is the first study to link functional and structural brain abnormalities in different types of dementia using data fusion. The results show that patients with AD and patients with BD exhibit similar brain changes in middle and posterior cingulate cortex, lingual gyrus, thalamus, thalamic radiation, Heschl's gyrus, and hippocampus, but also have distinct brain alterations in callosum, some superior frontal, and temporal regions. Our current work provides evidence of both commonalities and differences in functional brain connectivity and in WM integrity between the dementia groups, and point to the use of fusion analysis using multimodal features as a powerful tool for characterizing linked alterations in brain structure and function.

Acknowledgments

This work is supported by the National Institutes of Health (NIH) grants (1UH2NS100598-01, PI: Rosenberg; R01EB006841, R01REB020407, and P20GM103472, PI: Calhoun).

Appendix A. Supplementary data

Supplementary data to this article can be found online at https://doi.org/10.1016/j.nicl.2019.101937.

References

Alzheimer's, A., 2015. 2015 Alzheimer's disease facts and figures. Alzheimers Dement. 11, 332. https://doi.org/10.1016/j.jalz.2015.02.003.

Acosta-Cabronero, J., Alley, S., Williams, G.B., Pengas, G., Nestor, P.J., 2012. Diffusion tensor metrics as biomarkers in Alzheimer's disease. PLoS One 7, e49072. https://doi.org/10.1371/journal.pone.0049072.

Agosta, F., Pievani, M., Geroldi, C., Copetti, M., Frisoni, G.B., Filippi, M., 2012. Resting state fMRI in Alzheimer's disease: beyond the default mode network. Neurobiol. Aging 33, 1564–1578. https://doi.org/10.1016/j.neurobiolaging.2011.06.007.

Allen, G., Barnard, H., McColl, R., Hester, A.L., Fields, J.A., Weiner, M.F., Ringe, W.K., Lipton, A.M., Brooker, M., McDonald, E., 2007. Reduced hippocampal functional connectivity in Alzheimer disease. Arch. Neurol. 64, 1482–1487. https://doi.org/10.1001/archneur.64.10.1482.

Allen, E.A., Erhardt, E.B., Wei, Y., Eichele, T., Calhoun, V.D., 2012. Capturing inter-subject variability with group independent component analysis of fMRI data: a simulation study. Neuroimage. 59, 4141–4159. https://doi.org/10.1016/j.neuroimage.2011.10.010.

Allen, E.A., Damaraju, E., Plis, S.M., Erhardt, E.B., Eichele, T., Calhoun, V.D., 2014. Tracking whole-brain connectivity dynamics in the resting state. Cereb. Cortex 24, 663–676. https://doi.org/10.1093/cercor/bhs352.

Andersson, J.L., Skare, S., Ashburner, J., 2003. How to correct susceptibility distortions in spin-echo echo-planar images: application to diffusion tensor imaging. Neuroimage 20, 870–888. https://doi.org/10.1016/S1053-8119(03)00336-7.

Association, A. P, 2013. Diagnostic and Statistical Manual of Mental Disorders (DSM-5®). American Psychiatric Pub.

Bai, F., Liao, W., Watson, D.R., Shi, Y., Yuan, Y., Cohen, A.D., Xie, C., Wang, Y., Yue, C., Teng, Y., 2011. Mapping the altered patterns of cerebellar resting-state function in longitudinal amnestic mild cognitive impairment patients. J. Alzheimers Dis. 23, 87–99. https://doi.org/10.3233/JAD-2010-101533.

Bennett, D.A., Wilson, R.S., Gilley, D.W., Fox, J.H., 1990. Clinical diagnosis of Binswanger's disease. J. Neurol. Neurosurg. Psychiatry 53, 961–965. https://doi.org/10.1136/jnnp.53.11.961.

Bondi, M.W., Edmonds, E.C., Jak, A.J., Clark, L.R., Delano-Wood, L., McDonald, C.R., Nation, D.A., Libon, D.J., Au, R., Galasko, D., 2014. Neuropsychological criteria for mild cognitive impairment improves diagnostic precision, biomarker associations, and progression rates. J. Alzheimers Dis. 42, 275–289. https://doi.org/10.3233/JAD-140276.

Bookheimer, S.Y., Strojwas, M.H., Cohen, M.S., Saunders, A.M., Pericak-Vance, M.A.,

Mazziotta, J.C., Small, G.W., 2000. Patterns of brain activation in people at risk for Alzheimer's disease. N. Engl. J. Med. 343, 450–456. https://doi.org/10.1056/Nejm200008173430701.
Bozzali, M., Falini, A., Franceschi, M., Cercignani, M., Zuffi, M., Scotti, G., Comi, G., Filippi, M., 2002. White matter damage in Alzheimer's disease assessed in vivo using diffusion tensor magnetic resonance imaging. J. Neurol. Neurosurg. Psychiatry 72, 742–746. https://doi.org/10.1136/jnnp.72.6.742.
Calhoun, V.D., Sui, J., 2016. Multimodal fusion of brain imaging data: A key to finding the missing link (s) in complex mental illness. Biol. Psychiatry 1, 230–244. https://doi.org/10.1016/j.bpsc.2015.12.005.
Calhoun, V.D., Adali, T., Pearlson, G.D., Pekar, J., 2001. A method for making group inferences from functional MRI data using independent component analysis. Hum. Brain Mapp. 14, 140–151. https://doi.org/10.1002/Hbm.1048.
Calhoun, V., Adali, T., Giuliani, N., Pekar, J., Kiehl, K., Pearlson, G., 2006. Method for multimodal analysis of independent source differences in schizophrenia: combining gray matter structural and auditory oddball functional data. Hum. Brain Mapp. 27, 47–62. https://doi.org/10.1002/hbm.20166.
Calhoun, V.D., Liu, J., Adalı, T., 2009. A review of group ICA for fMRI data and ICA for joint inference of imaging, genetic, and ERP data. Neuroimage. 45, S163–S172. https://doi.org/10.1016/j.neuroimage.2008.10.057.
Castellazzi, G., Palesi, F., Casali, S., Vitali, P., Sinforiani, E., Wheeler-Kingshott, C.A., D'Angelo, E., 2014. A comprehensive assessment of resting state networks: bidirectional modification of functional integrity in cerebro-cerebellar networks in dementia. Front. Neurosci. 8, 223. https://doi.org/10.3389/fnins.2014.00223.
Celone, K.A., Calhoun, V.D., Dickerson, B.C., Atri, A., Chua, E.F., Miller, S.L., DePeau, K., Rentz, D.M., Selkoe, D.J., Blacker, D., 2006. Alterations in memory networks in mild cognitive impairment and Alzheimer's disease: an independent component analysis. J. Neurosci. 26, 10222–10231. https://doi.org/10.1523/JNEUROSCI.2250-06.2006.
Challis, E., Hurley, P., Serra, L., Bozzali, M., Oliver, S., Cercignani, M., 2015. Gaussian process classification of Alzheimer's disease and mild cognitive impairment from resting-state fMRI. Neuroimage. 112, 232–243. https://doi.org/10.1016/j.neuroimage.2015.02.037.
Chua, T.C., Wen, W., Slavin, M.J., Sachdev, P.S., 2008. Diffusion tensor imaging in mild cognitive impairment and Alzheimer's disease: a review. Curr. Opin. Neurol. 21, 83–92. https://doi.org/10.1097/WCO.0b013e3282f4594b.
Chui, H.C., 2007. Subcortical ischemic vascular dementia. Neurol. Clin. 25, 717–740. https://doi.org/10.1016/j.ncl.2007.04.003.
Correa, N.M., Li, Y.-O., Adali, T., Calhoun, V.D., 2008. Canonical correlation analysis for feature-based fusion of biomedical imaging modalities and its application to detection of associative networks in schizophrenia. IEEE J.Select. Topics Signal Process. 2, 998–1007. https://doi.org/10.1109/JSTSP.2008.2008265.
Correa, N.M., Adali, T., Li, Y.-O., Calhoun, V.D., 2010a. Canonical correlation analysis for data fusion and group inferences. IEEE Signal Process. Mag. 27, 39–50. https://doi.org/10.1109/MSP.2010.936725.
Correa, N.M., Eichele, T., Adalı, T., Li, Y.-O., Calhoun, V.D., 2010b. Multi-set canonical correlation analysis for the fusion of concurrent single trial ERP and functional MRI. Neuroimage. 50, 1438–1445. https://doi.org/10.1016/j.neuroimage.2010.01.062.
Corriveau, R.A., Bosetti, F., Emr, M., Gladman, J.T., Koenig, J.I., Moy, C.S., Pahigiannis, K., Waddy, S.P., Koroshetz, W., 2016. The science of vascular contributions to cognitive impairment and dementia (VCID): a framework for advancing research priorities in the cerebrovascular biology of cognitive decline. Cell. Mol. Neurobiol. 36, 281–288. https://doi.org/10.1007/s10571-016-0334-7.
Croitor-Sava, A., Martinez-Bisbal, M., Laudadio, T., Piquer, J., Celda, B., Heerschap, A., Sima, D., Van Huffel, S., 2011. Fusing in vivo and ex vivo NMR sources of information for brain tumor classification. Meas. Sci. Technol. 22, 114012. https://doi.org/10.1088/0957-0233/22/11/114012.
Dai, Z., Yan, C., Wang, Z., Wang, J., Xia, M., Li, K., He, Y., 2012. Discriminative analysis of early Alzheimer's disease using multi-modal imaging and multi-level characterization with multi-classifier (M3). Neuroimage. 59, 2187–2195. https://doi.org/10.1016/j.neuroimage.2011.10.003.
Damaraju, E., Allen, E., Belger, A., Ford, J., McEwen, S., Mathalon, D., Mueller, B., Pearlson, G., Potkin, S., Preda, A., 2014. Dynamic functional connectivity analysis reveals transient states of dysconnectivity in schizophrenia. NeuroImage Clin. 5, 298–308. https://doi.org/10.1016/j.nicl.2014.07.003.
Delbeuck, X., Van der Linden, M., Collette, F., 2003. Alzheimer'disease as a disconnection syndrome? Neuropsychol. Rev. 13, 79–92. https://doi.org/10.1023/A:1023832305702.
Douaud, G., Jbabdi, S., Behrens, T.E., Menke, R.A., Gass, A., Monsch, A.U., Rao, A., Whitcher, B., Kindlmann, G., Matthews, P.M., 2011. DTI measures in crossing-fibre areas: increased diffusion anisotropy reveals early white matter alteration in MCI and mild Alzheimer's disease. Neuroimage 55, 880–890. https://doi.org/10.1016/j.neuroimage.2010.12.008.
Du, Y., Fan, Y., 2013. Group information guided ICA for fMRI data analysis. Neuroimage. 69, 157–197. https://doi.org/10.1016/j.neuroimage.2012.11.008.
Du, Y., Allen, E.A., He, H., Sui, J., Wu, L., Calhoun, V.D., 2016. Artifact removal in the context of group ICA: A comparison of single-subject and group approaches. Hum. Brain Mapp. 37, 1005–1025. https://doi.org/10.1002/hbm.23086.
Dyrba, M., Grothe, M., Kirste, T., Teipel, S.J., 2015. Multimodal analysis of functional and structural disconnection in Alzheimer's disease using multiple kernel SVM. Hum. Brain Mapp. 36, 2118–2131. https://doi.org/10.1002/hbm.22759.
Engelhardt, E., Moreira, D.M., Alves, G.S., Lanna, M.E.O., Alves, C.E.D.O., Ericeira-Valente, L., Sudo, F.K., Laks, J., 2009. Binswanger's disease and quantitative fractional anisotropy. Arq. Neuropsiquiatr. 67, 179–184. https://doi.org/10.1590/S1980-57642009DN20400008.
Erhardt, E.B., Rachakonda, S., Bedrick, E.J., Allen, E.A., Adali, T., Calhoun, V.D., 2011. Comparison of multi-subject ICA methods for analysis of fMRI data. Hum. Brain Mapp. 32, 2075–2095. https://doi.org/10.1002/hbm.21170.
Erkinjuntti, T., 2002. Diagnosis and Management of Vascular Cognitive Impairment and Dementia. Springer, Stroke-Vascular Diseases, pp. 91–109.
Fazekas, F., Chawluk, J.B., Alavi, A., Hurtig, H.I., Zimmerman, R.A., 1987. MR signal abnormalities at 1.5 T in Alzheimer's dementia and normal aging. Am. J. Roentgenol. 149, 351–356. https://doi.org/10.2214/ajr.149.2.351.
Ferman, T.J., Smith, G.E., Kantarci, K., Boeve, B.F., Pankratz, V.S., Dickson, D.W., Graff-Radford, N.R., Wszolek, Z., Van Gerpen, J., Uitti, R., 2013. Nonamnestic mild cognitive impairment progresses to dementia with Lewy bodies. Neurology 81, 2032–2038. https://doi.org/10.1212/01.wnl.0000436942.55281.47.
Fu, Z., Tu, Y., Di, X., Du, Y., Pearlson, G., Turner, J., Biswal, B.B., Zhang, Z., Calhoun, V., 2017. Characterizing dynamic amplitude of low-frequency fluctuation and its relationship with dynamic functional connectivity: an application to schizophrenia. Neuroimage 180, 619–631. https://doi.org/10.1016/j.neuroimage.2017.09.035.
Fu, Z., Tu, Y., Di, X., Du, Y., Sui, J., Biswal, B.B., Zhang, Z., de Lacy, N., Calhoun, V., 2018. Transient increased thalamic-sensory connectivity and decreased whole-brain dynamism in autism. NeuroImage. https://doi.org/10.1016/j.neuroimage.2018.06.003.
Garrard, P., Maloney, L.M., Hodges, J.R., Patterson, K., 2004. The effects of very early Alzheimer's disease on the characteristics of writing by a renowned author. Brain 128, 250–260. https://doi.org/10.1093/brain/awh341.
Grady, C.L., McIntosh, A.R., Beig, S., Keightley, M.L., Burian, H., Black, S.E., 2003. Evidence from functional neuroimaging of a compensatory prefrontal network in Alzheimer's disease. J. Neurosci. 23, 986–993. https://doi.org/10.1523/JNEUROSCI.23-03-00986.2003.
Graña, M., Termenon, M., Savio, A., Gonzalez-Pinto, A., Echeveste, J., Pérez, J., Besga, A., 2011. Computer aided diagnosis system for Alzheimer disease using brain diffusion tensor imaging features selected by Pearson's correlation. Neurosci. Lett. 502, 225–229. https://doi.org/10.1016/j.neulet.2011.07.049.
Greicius, M.D., Srivastava, G., Reiss, A.L., Menon, V., 2004. Default-mode network activity distinguishes Alzheimer's disease from healthy aging: evidence from functional MRI. Proc. Natl. Acad. Sci. U. S. A. 101, 4637–4642. https://doi.org/10.1073/pnas.0308627101.
Greicius, M.D., Supekar, K., Menon, V., Dougherty, R.F., 2009. Resting-state functional connectivity reflects structural connectivity in the default mode network. Cereb. Cortex 19, 72–78. https://doi.org/10.1093/cercor/bhn059.
Henf, J., Grothe, M.J., Brueggen, K., Teipel, S., Dyrba, M., 2018. Mean diffusivity in cortical gray matter in Alzheimer's disease: the importance of partial volume correction. NeuroImage Clin. 17, 579–586. https://doi.org/10.1016/j.nicl.2017.10.005.
Himberg, J., Hyvarinen, A., 2003. Icasso: software for investigating the reliability of ICA estimates by clustering and visualization. In: 2003 IEEE XIII Workshop on Neural Networks for Signal Processing (IEEE Cat. No. 03TH8718). IEEE, pp. 259–268.
Hoptman, M.J., Zuo, X.-N., Butler, P.D., Javitt, D.C., D'Angelo, D., Mauro, C.J., Milham, M.P., 2010. Amplitude of low-frequency oscillations in schizophrenia: a resting state fMRI study. Schizophr. Res. 117, 13–20. https://doi.org/10.1016/j.schres.2009.09.030.
Huisa, B.N., Rosenberg, G.A., 2014. Binswanger's disease: toward a diagnosis agreement and therapeutic approach. Expert. Rev. Neurother. 14, 1203–1213. https://doi.org/10.1586/14737175.2014.956726.
Ibrahim, I., Horacek, J., Bartos, A., Hajek, M., Ripova, D., Brunovsky, M., Tintera, J., 2009. Combination of voxel based morphometry and diffusion tensor imaging in patients with Alzheimer's disease. Neuroendocrinol. Lett. 30, 39–45.
Jack, C.R., Bennett, D.A., Blennow, K., Carrillo, M.C., Dunn, B., Haeberlein, S.B., Holtzman, D.M., Jagust, W., Jessen, F., Karlawish, J., 2018. NIA-AA research framework: toward a biological definition of Alzheimer's disease. Alzheimers Dement. 14, 535–562. https://doi.org/10.1016/j.jalz.2018.02.018.
Jones, D., Machulda, M.M., Vemuri, P., McDade, E., Zeng, G., Senjem, M., Gunter, J., Przybelski, S., Avula, R., Knopman, D.S., 2011. Age-related changes in the default mode network are more advanced in Alzheimer disease. Neurology. 77, 1524–1531. https://doi.org/10.1212/WNL.0b013e318233b33d.
Jung, W.B., Lee, Y.M., Kim, Y.H., Mun, C.-W., 2015. Automated classification to predict the progression of Alzheimer's disease using whole-brain Volumetry and DTI. Psychiatry Investig. 12, 92–102. https://doi.org/10.4306/pi.2015.12.1.92.
Kalaria, R.N., Maestre, G.E., Arizaga, R., Friedland, R.P., Galasko, D., Hall, K., Luchsinger, J.A., Ogunniyi, A., Perry, E.K., Potocnik, F., 2008. Alzheimer's disease and vascular dementia in developing countries: prevalence, management, and risk factors. Lancet Neurol. 7, 812–826. https://doi.org/10.1016/S1474-4422(08)70169-8.
Kantarci, K., Jack Jr., C.R., Xu, Y.C., Campeau, N.G., O'Brien, P.C., Smith, G.E., Ivnik, R.J., Boeve, B.F., Kokmen, E., Tangalos, E.G., 2001. Mild cognitive impairment and Alzheimer disease: regional diffusivity of water. Radiology 219, 101–107. https://doi.org/10.1148/radiology.219.1.r01ap14101.
Kantarci, K., Avula, R., Senjem, M., Samikoglu, A., Zhang, B., Weigand, S., Przybelski, S., Edmonson, H.A., Vemuri, P., Knopman, D.S., 2010. Dementia with Lewy bodies and Alzheimer disease neurodegenerative patterns characterized by DTI. Neurology 74, 1814–1821. https://doi.org/10.1212/WNL.0b013e3181e0f7cf.
Kavcic, V., Ni, H., Zhu, T., Zhong, J., Duffy, C.J., 2008. White matter integrity linked to functional impairments in aging and early Alzheimer's disease. Alzheimer's Dementia 4, 381–389. https://doi.org/10.1016/j.jalz.2008.07.001.
Khazaee, A., Ebrahimzadeh, A., Babajani-Feremi, A., 2015. Identifying patients with Alzheimer's disease using resting-state fMRI and graph theory. Clin. Neurophysiol. 126, 2132–2141. https://doi.org/10.1016/j.clinph.2015.02.060.
Klaassens, B.L., van Gerven, J., van der Grond, J., de Vos, F., Möller, C., Rombouts, S.A., 2017. Diminished posterior precuneus connectivity with the default mode network differentiates normal aging from Alzheimer's disease. Front. Aging Neurosci. 9, 97. https://doi.org/10.3389/fnagi.2017.00097.
Lahat, D., Adali, T., Jutten, C., 2015. Multimodal data fusion: an overview of methods, challenges, and prospects. Proc. IEEE 103, 1449–1477. https://doi.org/10.1109/

Jproc.2015.2460697.
Li, Y.O., Adalı, T., Calhoun, V.D., 2007. Estimating the number of independent components for functional magnetic resonance imaging data. Hum. Brain Mapp. 28, 1251–1266. https://doi.org/10.1002/hbm.20359.
Li, Y.-O., Adali, T., Wang, W., Calhoun, V.D., 2009. Joint blind source separation by multiset canonical correlation analysis. IEEE Trans. Signal Process. 57, 3918–3929. https://doi.org/10.1109/Tsp.2009.2021636.
Li, Y.-D., Dong, H.-B., Xie, G.-M., Zhang, L.-j., 2013. Discriminative analysis of mild Alzheimer's disease and normal aging using volume of hippocampal subfields and hippocampal mean diffusivity: an in vivo magnetic resonance imaging study. Am. J. Alzheimers Dis. Other Dement. 28, 627–633. https://doi.org/10.1177/1533317513494452.
Loewenstein, D.A., Acevedo, A., Small, B.J., Agron, J., Crocco, E., Duara, R., 2009. Stability of different subtypes of mild cognitive impairment among the elderly over a 2-to 3-year follow-up period. Dement. Geriatr. Cogn. Disord. 27, 418–423. https://doi.org/10.1159/000211803.
Ma, S., Correa, N.M., Li, X.-L., Eichele, T., Calhoun, V.D., Adali, T., 2011. Automatic identification of functional clusters in FMRI data using spatial dependence. IEEE Trans. Biomed. Eng. 58, 3406–3417. https://doi.org/10.1109/Tbme.2011.2167149.
Mayo, C.D., Mazerolle, E.L., Ritchie, L., Fisk, J.D., Gawryluk, J.R., Initiative, A. s. D. N., 2017. Longitudinal changes in microstructural white matter metrics in Alzheimer's disease. NeuroImage Clin. 13, 330–338. https://doi.org/10.1016/j.nicl.2016.12.012.
McKhann, G., Drachman, D., Folstein, M., Katzman, R., Price, D., Stadlan, E.M., 1984. Clinical diagnosis of Alzheimer's disease report of the NINCDS-ADRDA Work Group* under the auspices of Department of Health and Human Services Task Force on Alzheimer's Disease. Neurology 34, 939. https://doi.org/10.1212/WNL.34.7.939.
McKhann, G.M., Knopman, D.S., Chertkow, H., Hyman, B.T., Jack Jr., C.R., Kawas, C.H., Klunk, W.E., Koroshetz, W.J., Manly, J.J., Mayeux, R., 2011. The diagnosis of dementia due to Alzheimer's disease: recommendations from the National Institute on Aging-Alzheimer's Association workgroups on diagnostic guidelines for Alzheimer's disease. Alzheimers Dement. 7, 263–269. https://doi.org/10.1016/j.jalz.2011.03.005.
O'reilly, J.X., Beckmann, C.F., Tomassini, V., Ramnani, N., Johansen-Berg, H., 2009. Distinct and overlapping functional zones in the cerebellum defined by resting state functional connectivity. Cereb. Cortex 20, 953–965. https://doi.org/10.1093/cercor/bhp157.
Parente, D.B., Gasparetto, E.L., da Cruz Jr., L.C., Domingues, R.C., Baptista, A.C., Carvalho, A.C., Domingues, R.C., 2008. Potential role of diffusion tensor MRI in the differential diagnosis of mild cognitive impairment and Alzheimer's disease. AJR Am. J. Roentgenol. 190, 1369–1374. https://doi.org/10.2214/AJR.07.2617.
Park, B.-Y., Kim, M., Seo, J., Lee, J.-M., Park, H., 2016. Connectivity analysis and feature classification in attention deficit hyperactivity disorder sub-types: a task functional magnetic resonance imaging study. Brain Topogr. 29, 429–439. https://doi.org/10.1007/s10548-015-0463-1.
Potkin, S., Turner, J., Brown, G., McCarthy, G., Greve, D., Glover, G., Manoach, D., Belger, A., Diaz, M., Wible, C., 2008. Working memory and DLPFC inefficiency in schizophrenia: the FBIRN study. Schizophr. Bull. 35, 19–31. https://doi.org/10.1093/schbul/sbn162.
Prasad, G., Joshi, S.H., Nir, T.M., Toga, A.W., Thompson, P.M., 2015. Brain connectivity and novel network measures for Alzheimer's disease classification. Neurobiol. Aging 36, S121–S131. https://doi.org/10.1016/j.neurobiolaging.2014.04.037.
Rashid, B., Damaraju, E., Pearlson, G.D., Calhoun, V.D., 2014. Dynamic connectivity states estimated from resting fMRI identify differences among schizophrenia, bipolar disorder, and healthy control subjects. Front. Hum. Neurosci. 8, 897. https://doi.org/10.3389/Fnhum.2014.00897.
Rashid, B., Arbabshirani, M.R., Damaraju, E., Cetin, M.S., Miller, R., Pearlson, G.D., Calhoun, V.D., 2016. Classification of schizophrenia and bipolar patients using static and dynamic resting-state fMRI brain connectivity. Neuroimage. 134, 645–657. https://doi.org/10.1016/j.neuroimage.2016.04.051.
Rose, S.E., Chen, F., Chalk, J.B., Zelaya, F.O., Strugnell, W.E., Benson, M., Semple, J., Doddrell, D.M., 2000. Loss of connectivity in Alzheimer's disease: an evaluation of white matter tract integrity with colour coded MR diffusion tensor imaging. J. Neurol. Neurosurg. Psychiatry 69, 528–530. https://doi.org/10.1136/jnnp.69.4.528.
Rose, S.E., Andrew, L., Chalk, J.B., 2008. Gray and white matter changes in Alzheimer's disease: a diffusion tensor imaging study. J. Magn. Reson. Imaging 27, 20–26. https://doi.org/10.1002/jmri.21231.
Rosenberg, G.A., 2017. Binswanger's disease: biomarkers in the inflammatory form of vascular cognitive impairment and dementia. J. Neurochem. 144, 634–643. https://doi.org/10.1111/jnc.14218.
Rosenberg, G.A., Wallin, A., Wardlaw, J.M., Markus, H.S., Montaner, J., Wolfson, L., Iadecola, C., Zlokovic, B.V., Joutel, A., Dichgans, M., 2016. Consensus statement for diagnosis of subcortical small vessel disease. J. Cereb. Blood Flow Metab. 36, 6–25. https://doi.org/10.1038/jcbfm.2015.172.
Rubinov, M., Sporns, O., 2010. Complex network measures of brain connectivity: uses and interpretations. Neuroimage. 52, 1059–1069. https://doi.org/10.1016/j.neuroimage.2009.10.003.
Salat, D., Tuch, D., Van der Kouwe, A., Greve, D., Pappu, V., Lee, S., Hevelone, N., Zaleta, A., Growdon, J., Corkin, S., 2010. White matter pathology isolates the hippocampal formation in Alzheimer's disease. Neurobiol. Aging 31, 244–256. https://doi.org/10.1016/j.neurobiolaging.2008.03.013.
Schmahmann, J.D., Weilburg, J.B., Sherman, J.C., 2007. The neuropsychiatry of the cerebellum—insights from the clinic. Cerebellum 6, 254–267. https://doi.org/10.1080/14734220701490995.
Soininen, H.S., Scbeltens, P., 1998. Early diagnostic indices for the prevention of Alzheimer's disease. Ann. Med. 30, 553–559. https://doi.org/10.3109/07853899809002604.
Sorg, C., Riedl, V., Mühlau, M., Calhoun, V.D., Eichele, T., Läer, L., Drzezga, A., Förstl, H., Kurz, A., Zimmer, C., 2007. Selective changes of resting-state networks in individuals at risk for Alzheimer's disease. Proc. Natl. Acad. Sci. 104, 18760–18765. https://doi.org/10.1073/pnas.0708803104.
Stahl, R., Dietrich, O., Teipel, S.J., Hampel, H., Reiser, M.F., Schoenberg, S.O., 2007. White matter damage in Alzheimer disease and mild cognitive impairment: assessment with diffusion-tensor MR imaging and parallel imaging techniques. Radiology. 243, 483–492. https://doi.org/10.1148/radiol.2432051714.
Stebbins, G., Murphy, C., 2009. Diffusion tensor imaging in Alzheimer's disease and mild cognitive impairment. Behav. Neurol. 21, 39–49. https://doi.org/10.3233/Ben-2009-0234.
Strittmatter, W.J., Saunders, A.M., Schmechel, D., Pericak-Vance, M., Enghild, J., Salvesen, G.S., Roses, A.D., 1993. Apolipoprotein E: high-avidity binding to beta-amyloid and increased frequency of type 4 allele in late-onset familial Alzheimer disease. Proc. Natl. Acad. Sci. 90, 1977–1981. https://doi.org/10.1073/pnas.90.5.1977.
Sui, J., Pearlson, G., Caprihan, A., Adali, T., Kiehl, K.A., Liu, J., Yamamoto, J., Calhoun, V.D., 2011. Discriminating schizophrenia and bipolar disorder by fusing fMRI and DTI in a multimodal CCA+ joint ICA model. Neuroimage 57, 839–855. https://doi.org/10.1016/j.neuroimage.2011.05.055.
Sui, J., Adali, T., Yu, Q., Chen, J., Calhoun, V.D., 2012. A review of multivariate methods for multimodal fusion of brain imaging data. J. Neurosci. Methods 204, 68–81. https://doi.org/10.1016/j.jneumeth.2011.10.031.
Sui, J., He, H., Pearlson, G.D., Adali, T., Kiehl, K.A., Yu, Q., Clark, V.P., Castro, E., White, T., Mueller, B.A., 2013. Three-way (N-way) fusion of brain imaging data based on mCCA+ jICA and its application to discriminating schizophrenia. NeuroImage. 66, 119–132. https://doi.org/10.1016/j.neuroimage.2012.10.051.
Sui, J., Pearlson, G.D., Du, Y., Yu, Q., Jones, T.R., Chen, J., Jiang, T., Bustillo, J., Calhoun, V.D., 2015. In search of multimodal neuroimaging biomarkers of cognitive deficits in schizophrenia. Biol. Psychiatry 78, 794–804. https://doi.org/10.1016/j.biopsych.2015.02.017.
Tucholka, A., Grau-Rivera, O., Falcon, C., Rami, L., Sánchez-Valle, R., Lladó, A., Gispert, J.D., Molinuevo, J.L., Initiative, A. s. D. N., 2018. Structural connectivity alterations along the Alzheimer's disease continuum: reproducibility across two independent samples and correlation with cerebrospinal fluid amyloid-β and tau. J. Alzheimers Dis. 61, 1575–1587. https://doi.org/10.3233/JAD-170553.
Turner, J.A., Damaraju, E., Van Erp, T.G., Mathalon, D.H., Ford, J.M., Voyvodic, J., Mueller, B.A., Belger, A., Bustillo, J., McEwen, S.C., 2013. A multi-site resting state fMRI study on the amplitude of low frequency fluctuations in schizophrenia. Front. Neurosci. 7, 137. https://doi.org/10.3389/fnins.2013.00137.
Venneri, A., McGeown, W.J., Hietanen, H.M., Guerrini, C., Ellis, A.W., Shanks, M.F., 2008. The anatomical bases of semantic retrieval deficits in early Alzheimer's disease. Neuropsychologia. 46, 497–510. https://doi.org/10.1016/j.neuropsychologia.2007.08.026.
Wang, L., Zang, Y., He, Y., Liang, M., Zhang, X., Tian, L., Wu, T., Jiang, T., Li, K., 2006. Changes in hippocampal connectivity in the early stages of Alzheimer's disease: evidence from resting state fMRI. Neuroimage. 31, 496–504. https://doi.org/10.1016/j.neuroimage.2005.12.033.
Wang, K., Liang, M., Wang, L., Tian, L., Zhang, X., Li, K., Jiang, T., 2007. Altered functional connectivity in early Alzheimer's disease: a resting-state fMRI study. Hum. Brain Mapp. 28, 967–978. https://doi.org/10.1002/hbm.20324.
Wu, X., Li, J., Ayutyanont, N., Protas, H., Jagust, W., Fleisher, A., Reiman, E., Yao, L., Chen, K., 2013. The receiver operational characteristic for binary classification with multiple indices and its application to the neuroimaging study of Alzheimer's disease. IEEE/ACM Trans. Comput. Biol. Bioinforma. 10, 173–180. https://doi.org/10.1109/TCBB.2012.141.
Yetkin, F.Z., Rosenberg, R.N., Weiner, M.F., Purdy, P.D., Cullum, C.M., 2006. FMRI of working memory in patients with mild cognitive impairment and probable Alzheimer's disease. Eur. Radiol. 16, 193–206. https://doi.org/10.1007/s00330-005-2794-x.
Yin, X., Liu, C., Gui, L., Zhao, L., Zhang, J., Wei, L., Xie, B., Zhou, D., Li, C., Wang, J., 2014. Comparison of medial temporal measures between Binswanger's disease and Alzheimer's disease. PLoS One 9, e86423. https://doi.org/10.1371/journal.pone.0086423.
Zhao, Q., Lu, H., Metmer, H., Li, W.X., Lu, J., 2018. Evaluating functional connectivity of executive control network and frontoparietal network in Alzheimer's disease. Brain Res. 1678, 262–272. https://doi.org/10.1016/j.brainres.2017.10.025.
Zheng, W., Liu, X., Song, H., Li, K., Wang, Z., 2017. Altered functional connectivity of cognitive-related cerebellar subregions in Alzheimer's disease. Front. Aging Neurosci. 9, 143. https://doi.org/10.3389/Fnagi.2017.00143.
Zhou, J., Greicius, M.D., Gennatas, E.D., Growdon, M.E., Jang, J.Y., Rabinovici, G.D., Kramer, J.H., Weiner, M., Miller, B.L., Seeley, W.W., 2010. Divergent network connectivity changes in behavioural variant frontotemporal dementia and Alzheimer's disease. Brain. 133, 1352–1367. https://doi.org/10.1093/brain/awq075.
Zhu, Q.-Y., Bi, S.-W., Yao, X.-T., Ni, Z.-Y., Li, Y., Chen, B.-Y., Fan, G.-G., Shang, X.-L., 2015. Disruption of thalamic connectivity in Alzheimer's disease: a diffusion tensor imaging study. Metab. Brain Dis. 30, 1295–1308. https://doi.org/10.1007/s11011-015-9708-7.